Design of a High Misalignment Tolerance and CV Output WPT System Using a Secondary Repeater

Yingjie Li, Zhiping Zuo, Fengwei Chen, Chunsen Tang, Jing Xiao, and Shaonan Chen

***Abstract*—This article is dedicated to improving the misalignment tolerance of a wireless power transfer (WPT) system using a secondary repeater. To mitigate the drop of mutual inductance when misalignment occurs, the receiver with a co-axial intermediate coil is deployed. As such, the proposed system contains three tuning ratios which correspond to the transmitting, intermediate, and receiving coils. To facilitate the choice of these parameters, an efficient tuning technique is proposed. With the proposed tuning technique, one can conveniently achieve zero voltage switching, constant voltage output, load power regulation, and suppression of load voltage fluctuation under coil misalignment. A 500-W experimental prototype is built to verify the effectiveness and superiority of the secondary intermediate aided (SIA) system. The experimental results show that within a 80-mm planar misalignment range (53.3% of the primary coil diameter), the output voltage fluctuation of the SIA WPT system is within 3%, and the peak dc–dc efficiency is 86.87%. In the vertical transfer distance range of 30–65 mm (70% of the standard transfer distance), the output voltage fluctuation is within 5%, with a peak dc–dc efficiency of 88.27%.**

***Index Terms*—Constant voltage output, intermediate aided coil, misalignment tolerance, tuning method, wireless power transfer (WPT).**

I. Introduction

WIRELESS power transfer (WPT) has been gaining popularity due to its advantages of high security, high reliability, and high flexibility [1], [2], [3], [4]. As a new power transfer technology, it has been widely applied in robotics, biomedical implantation, consumer electronics, household appliances, electric vehicles, and underwater equipment [5], [6], [7], [8], [9], [10], [11], [12]. In practical applications, the receiver is often located on movable electrical devices, making it difficult to achieve precise alignment between the transmitter and receiver during the charging process. This misalignment can cause changes in their mutual inductance, leading to instability in transfer power, efficiency, output voltage and current, etc. Therefore, misalignment tolerance is a crucial indicator for evaluating the performance of WPT systems.

Numerous methods have been proposed to improve the misalignment tolerance of WPT systems. Several pads, such as Double-D [13], double-D quadrature pad [14], bipolar pad [15], and flat solenoid pad [16], have been designed to improve misalignment tolerance in one direction by creating a uniform magnetic field. However, these approaches only improve the misalignment tolerance of the system in one direction, while the misalignment tolerance in other directions remains unchanged. To overcome this problem, other pads, such as H-shaped coupler [17], third-coil [18], solenoid and double-D pad [19], and split flat solenoid coupler [20] have been designed to improve the misalignment tolerance along the x and y directions by using multiple coils to compensate for the magnetic field.

To further improve misalignment tolerance, some compensation topologies, such as a dual-coupled double LCC compensation, X-type compensation, and PS/S compensation have been investigated in [21], [22], and [23]. Furthermore, LCL and CL are connected in parallel on the primary and secondary sides, and the series inductors of the primary and pick-up LCL networks, while LCC-S and S-LCC based hybrid IPT topology using the ISOP structure, have been adopted in [24], [25], and [26]. Although these topologies improve misalignment tolerance in multiple directions, they introduce greater complexity into the system. Meanwhile, the misalignment tolerance can also be improved by control algorithms. For example, in [27] and [28], a multivariable control strategy and a variable frequency controller are presented to improve misalignment tolerance. It should be noted that, although these control methods are able to stabilize the system output and improve misalignment tolerance, they inevitably introduce higher computational burden, and so are not suitable for implementation on cost-sensitive processors.

Intermediate coils are another way to improve the misalignment tolerance for WPT systems. In [29], two intermediate coils are placed outside the transmitter and receiver to the coupling area in x and y directions, but this approach greatly increases the size of the coupler. In [30], an intermediate coil located at the transmitter operates in both repeater-aided mode and power-interactive mode, thereby improving planar misalignment tolerance. However, the additional inverters introduced in power-interactive mode still significantly increase the overall size of the system, and the switching between the two modes makes the control more complicated.

Received 9 April 2025; revised 27 May 2025; accepted 27 June 2025. Date of publication 2 July 2025; date of current version 27 August 2025. This work was supported in part by the National Natural Science Foundation of China under Grant 62073246 and in part by the Fundamental Research Funds for the Central Universities under Grant 2024CDJGF-015. Recommended for publication by Associate Editor X. Ruan. *(Corresponding author: Zhiping Zuo.)*

Yingjie Li, Zhiping Zuo, Fengwei Chen, and Chunsen Tang are with the School of Automation, Chongqing University, Chongqing 400044, Chongqing (e-mail: 20221301006@stu.cqu.edu.cn; zpzuo@cqu.edu.cn; fengwei.chen@cqu.edu.cn; cstang@cqu.edu.cn).

Jing Xiao and Shaonan Chen are with the Southern Power Grid Corporation Wireless Power Transmission Joint Laboratory Chongqing University Chongqing, Nanning, Guangxi 530023, China (e-mail: xiao_j.sy@gx.csg.cn; chen_sn.sy@gx.csg.cn).

Color versions of one or more figures in this article are available at https://doi.org/10.1109/TPEL.2025.3585252.

Digital Object Identifier 10.1109/TPEL.2025.3585252

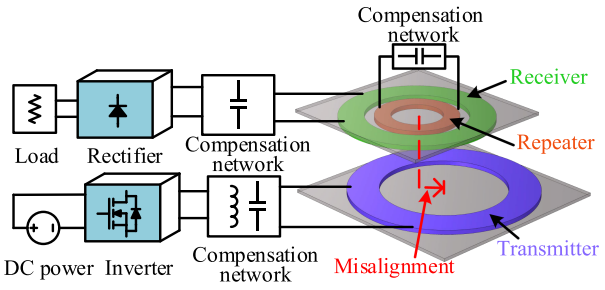

Fig. 1. Structure of the proposed intermediate aided WPT system.

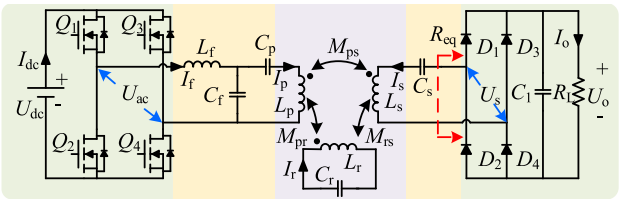

Fig. 2. Structure of the proposed intermediate aided WPT system.

Considering the challenges of previous technologies, this article considers using a secondary passive co-axial intermediate-aided coil to improve the misalignment tolerance for a wireless power transfer system, and a tuning method is proposed to design an LCC-S-S compensation WPT system. In this system, the output is influenced by transmitter coil tuning ratio β, intermediate-aided coil tuning ratio γ, and receiver coil tuning ratio δ. Specifically, the stability and amplitude of the system output are influenced by the intermediate-aided coil tuning ratio γ and the receiver coil tuning ratio δ, while the zero voltage switching (ZVS) of the inverter is predominantly influenced by the transmitter coil tuning ratio β. By appropriately designing the coupler and tuning ratios β, γ, and δ, the system output can be maximized and remains constant in a large misalignment range, and ZVS is guaranteed. Compared with the existing approaches, the proposed approach neither introduces complex control algorithms and system structures, nor increases the size of the coupler.

The rest of this article is organized as follows. Section II introduces the structure of the SIA WPT system and establishes its model. In Section III, the tuning method using a secondary intermediate-aided coil is proposed to improve misalignment tolerance. In Section IV, a 500 W prototype is constructed to verify the theoretical analysis. Finally, Section V concludes this article.

II. System Modeling and Intermediate Aided Coil Position Analyzing

A. System Modeling With Intermediate Aided Coil

The WPT system considered in this article is sketched in Fig. 1, and its equivalent circuit is shown in Fig. 2, with the parameters in Fig. 2 listed in Table I. The dc power is converted to high frequency ac power via an inverter composed of Q_1–Q_4. Then, this ac power is fed to a parallel resonator composed of L_f and C_f. Subsequently, the voltage on C_f is used to transfer power, which generates ac magnetic field through the transmitting coil (Tx). This forms the so-called LCC compensation network, in which C_f is used to match the impedance. Next, the induced voltage excited by a triple coupling formed between the Tx, the receiving coil (Rx), and the intermediate aided coil (Ix) located at the receiver for power transfer. After that, the high frequency ac induced voltage in the secondary coil is converted to dc voltage via a rectifier consisting of D_1–D_4 and supplied to the load. In this article, misalignment is defined as the positional deviation between the center of receiver and the center of transmitter as described in Fig. 1. To reduce reactive power loss and improve transfer efficiency, compensation capacitors C_r and C_s are connected in series with the Ix and Rx.

TABLE I
Specification of the Proposed System

Specification	Symbol
DC input voltage, current	U_{dc}, I_{dc}
Converter output voltage,current	U_{ac}, I_f
Current in coils Tx, Ix, Rx	I_p, I_r, I_s
Rectifier input voltage	U_s
DC output voltage, current	U_o, I_o
DC output filtering capacitor	C_1
Inductance of Tx, Ix, Rx	L_p, L_r, L_s
Mutual inductance between Tx, Ix, Rx	M_{ps}, M_{pr}, M_{rs}
Compensation capacitance of Tx, Ix, Rx	C_p, C_r, C_s
Filter inductance and capacitance of LCC	L_f, C_f
Output equivalent load and dc load	R_{eq}, R_L

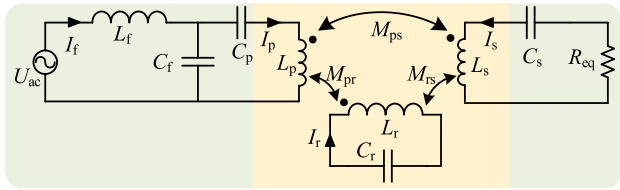

Fig. 3. Simplified circuit model of the intermediate aided system.

To analyze the principle of the SIA WPT system proposed in this article, the equivalent circuit shown in Fig. 2 is simplified as Fig. 3. For ease of analysis, the equivalent series resistances of the coils will be ignored in the rest of the article.

To analyze the impact of each circuit component in the circuit on the system performance, let us define the following notations:

$$\begin{cases} Z_1 = j\omega L_f, Z_2 = \frac{1}{j\omega C_f}, Z_3 = j\omega L_p, Z_4 = \frac{1}{j\omega C_p}, \\ Z_r = j\omega L_r + \frac{1}{j\omega C_r}, Z_s = j\omega L_s + \frac{1}{j\omega C_s} + R_{eq}. \end{cases} \tag{1}$$

According to Kirchhoff's law, the system can be described by the following equations:

$$\begin{bmatrix} Z_1+Z_2 & -Z_2 & 0 & 0 \\ -Z_2 & Z_3+Z_4+Z_2 & j\omega M_{pr} & j\omega M_{ps} \\ 0 & j\omega M_{pr} & Z_r & j\omega M_{rs} \\ 0 & j\omega M_{ps} & j\omega M_{rs} & Z_s \end{bmatrix} \begin{bmatrix} \dot{I}_f \\ \dot{I}_p \\ \dot{I}_r \\ \dot{I}_s \end{bmatrix} = \begin{bmatrix} \dot{U}_{ac} \\ 0 \\ 0 \\ 0 \end{bmatrix} \tag{2}$$

where ω is the angular operating frequency. Substituting (1) into (2), we can obtain

$$\begin{cases} \dot{I}_{\mathrm{f}} = \dot{U}_{\mathrm{ac}} B/A \\ \dot{I}_{\mathrm{p}} = \dot{U}_{\mathrm{ac}} Z_2(\omega^2 M_{\mathrm{rs}}^2 + Z_{\mathrm{r}} Z_{\mathrm{s}})/A \\ \dot{I}_{\mathrm{r}} = -\dot{U}_{\mathrm{ac}} j\omega Z_2(M_{\mathrm{pr}} Z_{\mathrm{s}} - j\omega M_{\mathrm{ps}} M_{\mathrm{rs}})/A \\ \dot{I}_{\mathrm{s}} = -\dot{U}_{\mathrm{ac}} j\omega Z_2(j\omega M_{\mathrm{pr}} M_{\mathrm{rs}} - M_{\mathrm{ps}} Z_{\mathrm{r}})/A \end{cases} \tag{3}$$

where

$$\begin{aligned} A &= (\omega^2 M_{\mathrm{ps}}^2 Z_{\mathrm{r}} + \omega^2 M_{\mathrm{pr}}^2 Z_{\mathrm{s}} - 2j\omega^3 M_{\mathrm{ps}} M_{\mathrm{pr}} M_{\mathrm{rs}})(Z_1 + Z_2) \\ &\quad + (\omega^2 M_{\mathrm{rs}}^2 + Z_{\mathrm{r}} Z_{\mathrm{s}})(Z_1 Z_2 + Z_1 Z_3 + Z_1 Z_4 + Z_2 Z_3 + Z_2 Z_4) \\ B &= \omega^2 (M_{\mathrm{ps}}^2 Z_{\mathrm{r}} + M_{\mathrm{pr}}^2 Z_{\mathrm{s}}) + (\omega^2 M_{\mathrm{rs}}^2 + Z_{\mathrm{r}} Z_{\mathrm{s}})(Z_2 + Z_3 + Z_4) \\ &\quad - 2j\omega^3 M_{\mathrm{ps}} M_{\mathrm{pr}} M_{\mathrm{rs}}. \end{aligned}$$

Subsequently, let us define the tuning ratios of the filter inductance L_{f}, Tx, Ix, and Rx, as α, β, γ, and δ, respectively. They satisfy the following relations:

$$\begin{cases} Z_1 + Z_2 = \alpha Z_1, Z_2 + Z_3 + Z_4 = \beta Z_3, \\ Z_{\mathrm{r}} = \gamma j\omega L_r, Z_{\mathrm{s}} = \delta j\omega L_{\mathrm{s}} + R_{\mathrm{eq}} \end{cases}. \tag{4}$$

Normally, L_{f} and C_{f} are operated at the resonant state, indicating that $\alpha = 0$. Substituting (4) into (3) leads to

$$\begin{cases} \dot{I}_{\mathrm{f}} = -\frac{\dot{U}_{\mathrm{ac}} B}{j\omega L_{\mathrm{f}}^2 A} \\ \dot{I}_{\mathrm{p}} = \dot{U}_{\mathrm{ac}}/(j\omega L_{\mathrm{f}}) \\ \dot{I}_{\mathrm{r}} = -\frac{\dot{U}_{\mathrm{ac}}[\omega(\delta L_{\mathrm{s}} M_{\mathrm{pr}} - M_{\mathrm{ps}} M_{\mathrm{rs}}) - jR_{\mathrm{eq}} M_{\mathrm{pr}}]}{j\omega L_{\mathrm{f}} A} \\ \dot{I}_{\mathrm{s}} = \dot{U}_{\mathrm{ac}}(M_{\mathrm{rs}} M_{\mathrm{pr}} - \gamma L_{\mathrm{r}} M_{\mathrm{ps}})/(L_{\mathrm{f}} A) \end{cases} \tag{5}$$

where

$$\begin{aligned} A &= \gamma R_{\mathrm{eq}} L_{\mathrm{r}} + j\omega(\gamma\delta L_{\mathrm{r}} L_{\mathrm{s}} - M_{\mathrm{rs}}^2) \\ B &= (\omega\gamma\beta\delta L_{\mathrm{p}} L_{\mathrm{r}} L_{\mathrm{s}} - j\beta\gamma L_{\mathrm{p}} L_{\mathrm{r}} R_{\mathrm{eq}} - \omega\beta L_{\mathrm{p}} M_{\mathrm{rs}}^2 \\ &\quad - \omega\gamma L_{\mathrm{r}} M_{\mathrm{ps}}^2 - \omega\delta L_{\mathrm{s}} M_{\mathrm{pr}}^2 + jM_{\mathrm{pr}}^2 R_{\mathrm{eq}} + 2\omega M_{\mathrm{ps}} M_{\mathrm{pr}} M_{\mathrm{rs}}). \end{aligned}$$

The output voltage on the ac side can be expressed as

$$\dot{U}_{\mathrm{s}} = \dot{I}_{\mathrm{s}} R_{\mathrm{eq}} = \frac{\dot{U}_{\mathrm{ac}}(M_{\mathrm{pr}} M_{\mathrm{rs}} - \gamma L_{\mathrm{r}} M_{\mathrm{ps}}) R_{\mathrm{eq}}}{L_{\mathrm{f}} A} \tag{6}$$

while the output power is expressed as

$$P_{\mathrm{out}} = |\dot{U}_{\mathrm{s}}||\dot{I}_{\mathrm{s}}| \cos(\theta) = \frac{U_{\mathrm{ac}}^2 (M_{\mathrm{pr}} M_{\mathrm{rs}} - \gamma L_{\mathrm{r}} M_{\mathrm{ps}})^2 R_{\mathrm{eq}}^2}{L_{\mathrm{f}}^2 A^2}. \tag{7}$$

B. Influence of Intermediate Aided Coil Position

In this article, the topology of the system takes the transmitter–receiver mode, which means that the Ix can be placed either at the transmitter or the receiver. It should be noted that the placement of the Ix could greatly affect the performance of the system. In the following, the output characteristics of the system in the two configurations will be analyzed.

1) Intermediate Aided Coil Located At Transmitter: When the Ix is located at the transmitter, the relative position between the Tx and the Ix is fixed. In this situation, when misalignment occurs, M_{pr} remains constant, while M_{rs} and M_{ps} could vary with respect to position. For simplicity of analysis, the Tx and Ix are designed such that $L_{\mathrm{p}} = L_{\mathrm{r}}$, $M_{\mathrm{rs}} = M_{\mathrm{ps}}$ in perfect alignment, and $M_{\mathrm{rs}} = M_{\mathrm{ps}}$ with misalignment. In this case, $\dot{I}_{\mathrm{s}}$ can be expressed as

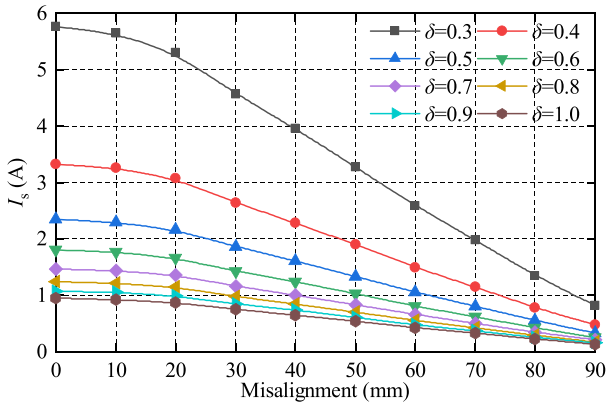

Fig. 4. Variation of I_{s} against misalignment when Ix placed at transmitter.

$$\dot{I}_{\mathrm{s}} = \frac{\dot{U}_{\mathrm{ac}} M_{\mathrm{rs}}(M_{\mathrm{pr}} - \gamma L_{\mathrm{r}})}{L_{\mathrm{f}}[\gamma R_{\mathrm{eq}} L_{\mathrm{r}} + j\omega(\gamma\delta L_{\mathrm{r}} L_{\mathrm{s}} - M_{\mathrm{rs}}^2)]} \tag{8}$$

where I_{s} is the amplitude of $\dot{I}_{\mathrm{s}}$, which is expressed as

$$I_{\mathrm{s}} = \frac{U_{\mathrm{ac}} M_{\mathrm{rs}} |M_{\mathrm{pr}} - \gamma L_{\mathrm{r}}|}{L_{\mathrm{f}} \sqrt{\left[\gamma^2 R_{\mathrm{eq}}^2 L_{\mathrm{r}}^2 + \omega^2 (M_{\mathrm{rs}}^2 - \gamma\delta L_{\mathrm{r}} L_{\mathrm{s}})^2\right]}}. \tag{9}$$

To simplify the analysis of $\dot{I}_{\mathrm{s}}$ when misalignment occurs, let $\gamma = 0$, and I_{s} can be expressed as

$$I_{\mathrm{s}} = \left| \frac{U_{\mathrm{ac}} M_{\mathrm{pr}}}{\omega L_{\mathrm{f}} M_{\mathrm{rs}}} \right|. \tag{10}$$

The variation of I_{s} against misalignment is shown in Fig. 4, where it can be seen that when δ is in the range [0.3, 1], and I_{s} cannot remain constant in the considered misalignment range. This means that when the Ix is placed at the transmitter, the system's misalignment tolerance cannot be improved.

2) Intermediate Aided Coil Located At Receiver: When the Ix is placed at the receiver, the relative position between the Rx and the Ix is fixed. When misalignment occurs, M_{rs} remains constant, while M_{pr} and M_{ps} could vary with respect to position. As U_{ac}, M_{rs}, ω, L_{f}, δ, and L_{s} are constant against misalignment, according to (5), A decouples with misalignment when Ix is placed at the receiver. To achieve a constant output current I_{s} against misalignment under the same R_{eq}, the following term should be a constant:

$$M_{\mathrm{rs}} M_{\mathrm{pr}} - \gamma L_{\mathrm{r}} M_{\mathrm{ps}}. \tag{11}$$

Under perfect alignment, the mutual inductance between Tx and Rx is $M_{\mathrm{ps},0}$, while the mutual inductance between Tx and Ix is $M_{\mathrm{pr},0}$. When misalignment occurs, the variations in mutual inductance are denoted as ΔM_{ps} and ΔM_{pr}, then (11) is expressed as

$$M_{\mathrm{pr},0} M_{\mathrm{rs},0} - \gamma L_{\mathrm{r}} M_{\mathrm{ps},0} + \Delta M_{\mathrm{pr}} M_{\mathrm{rs}} - \gamma L_{\mathrm{r}} \Delta M_{\mathrm{ps}}. \tag{12}$$

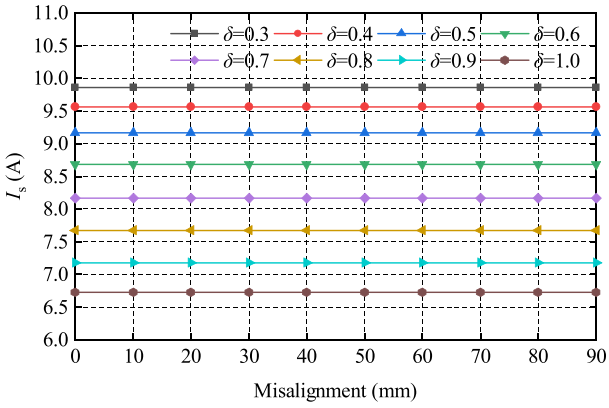

Fig. 5. Variation of I_s against misalignment when Ix placed at receiver.

To ensure that (11) is constant, we need to further impose

$$\Delta M_{pr} M_{rs} - \gamma L_r \Delta M_{ps} = 0 \tag{13}$$

which can be equivalently written as

$$\frac{\gamma L_r}{M_{rs}} = \frac{\Delta M_{pr}}{\Delta M_{ps}}. \tag{14}$$

According to (14), when ΔM_{ps} and ΔM_{pr} vary linearly, the value of (11) remains constant throughout the misalignment. As stated in [18] and [19], it is possible to maintain a linear relationship between ΔM_{ps} and ΔM_{pr} during a misalignment process. In the case of $\Delta M_{ps} = \Delta M_{pr}$, the variation of I_s against misalignment is shown in Fig. 5, where it is evident that I_s is a constant value during the misalignment process, therefore the intermediate coil placed at the receiver can enhance the system's misalignment tolerance under certain conditions.

In summary, when the Ix is placed at the transmitter, the output current I_s cannot remain constant. However, by placing the Ix at the receiver, designing coupler and Ix tuning ratio γ can achieve constant I_s during misalignment. Therefore, in this article, the Ix will be placed at the receiver, and the method for designing the coupling mechanism and tuning the coil parameters are specifically described in the next subsection.

III. Tuning Method and Coupler Analysis

A. Tuning Method

Generally, coil tuning can reduce reactive power loss and improve transfer efficiency, but the commonly used tuning method for two-coil system is not applicable to the SIA WPT system. Therefore, this section will analyze the tuning method specific to the SIA WPT system.

According to (5), when the Ix is placed at the receiver, the output current I_s on the ac side can be a constant value during misalignment by designing the Ix and adjusting Ix tuning ratio γ. The role of δ is to achieve the system's maximum power transfer and to decouple the output voltage from the load, while the inverter voltage and current phase can be adjusted by modifying Tx tuning ratio β. The primary objective of this article is to improve the misalignment tolerance of the WPT system, followed by achieving constant output voltage, maximizing power transfer, and ensuring the ZVS state of the inverter. Therefore, in this article, the primary focus is on the Ix tuning ratio γ, followed by an analysis of the Rx tuning ratio δ and the Tx tuning ratio β.

1) Design Intermediate Aided Coil Tuning Ratio γ: The Ix can be designed to operate in inductive, capacitive, or resonant states, and the system characteristics vary depending on the state of the intermediate coil. However, the primary objective of this article is to improve the system's misalignment tolerance; therefore, the design of the Ix tuning ratio γ is crucial. Since the γ is determined by $\Delta M_{pr}/\Delta M_{ps}$, therefore, before designing γ, we need to determine $\Delta M_{pr}/\Delta M_{ps}$.

Based on the previous analysis, the coupler needs to be designed so that ΔM_{ps} and ΔM_{pr} satisfy the following relationship:

$$\Delta M_{pr} = a \Delta M_{ps} \tag{15}$$

where a is a constant representing the ratio of the mutual inductance variation $\Delta M_{pr}/\Delta M_{ps}$ during the misalignment process. With this definition, (14) can be rewritten as

$$\gamma = a M_{rs}/L_r \tag{16}$$

Eq. (5) is further expressed as

$$\begin{cases} \dot{I}_f = -\frac{\dot{U}_{ac} B}{j\omega L_f^2 A} \\ \dot{I}_p = \dot{U}_{ac}/(j\omega L_f) \\ \dot{I}_r = -\frac{\dot{U}_{ac}[\omega(\delta L_s M_{pr} - M_{ps} M_{rs}) - j R_{eq} M_{pr}]}{j\omega L_f A} \\ \dot{I}_s = \frac{\dot{U}_{ac} M_{rs}(M_{pr} - a M_{ps})}{L_f A} \end{cases} \tag{17}$$

where A and B are further expressed as

$$A = M_{rs}\left[a R_{eq} + j\omega(a\delta L_s - M_{rs})\right]$$

$$B = a\omega\beta\delta L_p L_s M_{rs} - aj\beta L_p R_{eq} M_{rs} - \omega\beta L_p M_{rs}^2 - a\omega M_{rs} M_{ps}^2 - \omega\delta L_s M_{pr}^2 + j M_{pr}^2 R_{eq} + 2\omega M_{ps} M_{pr} M_{rs}.$$

To simplify the analysis, the mutual inductance is equivalently transformed as follows:

$$M_{eq} = M_{pr} - a M_{ps}. \tag{18}$$

2) Design Receiving Coil Tuning Ratio δ: According to (17), I_s can be adjusted by tuning δ to control its amplitude and phase. The current of the Rx and output voltage, and the output power P_{out} are given by

$$\dot{I}_s = \frac{\dot{U}_{ac} M_{eq}}{L_f} \frac{a R_{eq} - j\omega(M_{rs} - a\delta L_s)}{a^2 R_{eq}^2 + \omega^2 (M_{rs} - a\delta L_s)^2} \tag{19}$$

$$I_s = \frac{U_{ac} M_{eq}}{L_f \sqrt{a^2 R_{eq}^2 + \omega^2 (M_{rs} - a\delta L_s)^2}} \tag{20}$$

$$U_s = \frac{U_{ac} M_{eq} R_{eq}}{L_f \sqrt{a^2 R_{eq}^2 + \omega^2 (M_{rs} - a\delta L_s)^2}} \tag{21}$$

$$P_{out} = I_s^2 R_{eq} = \frac{U_{ac}^2 M_{eq}^2 R_{eq}}{L_f^2 [a R_{eq} + j\omega M_{rs}(M_{rs} - \delta L_s)]^2}. \tag{22}$$

According to (20), the Rx tuning ratio δ affects the amplitude of the current I_s for the same R_{eq}. According to (21), both the Rx

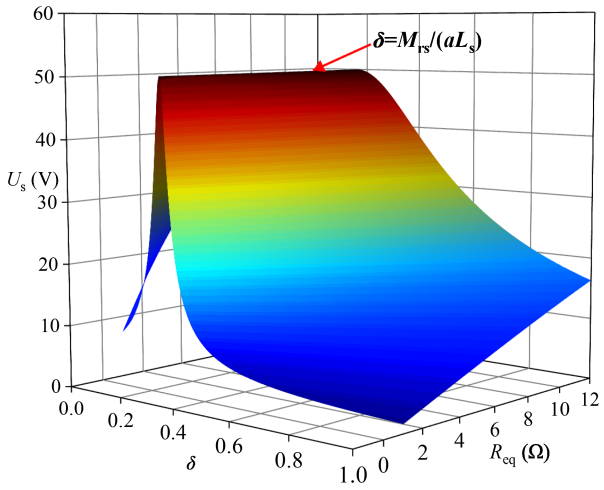

Fig. 6. Variation of U_s with different values of δ and R_{eq}.

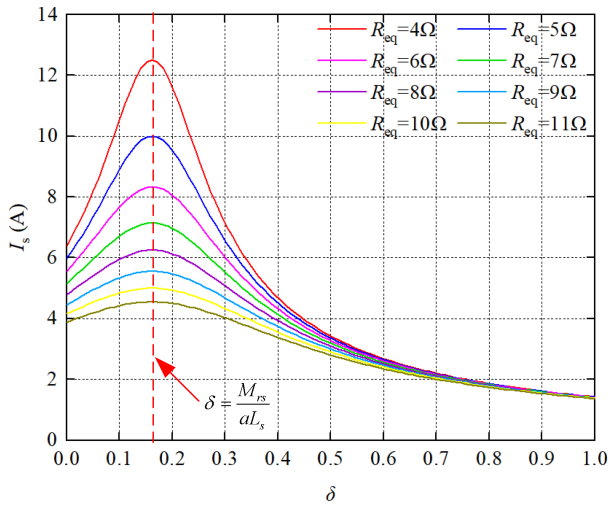

Fig. 7. Variation of I_s with misalignment for different value of δ.

tuning ratio δ and R_{eq} affect the voltage U_s. According to (22), the Rx tuning ratio δ affects the output power for a given R_{eq} and output voltage U_s. To achieve both a constant output voltage U_s and maximum power across different R_{eq}, δ must be adjusted appropriately to maintain a constant output voltage U_s and maximize the amplitude of I_s. The variation of U_s with different δ and R_{eq} is shown in Fig. 6, where it can be seen that, when $\delta = M_{rs}/(aL_s)$, the output voltage U_s remains constant with different resistance R_{eq}, achieving a constant voltage output. The variation of I_s with δ under different loads is shown in Fig. 7. From Fig. 7, the amplitude of I_s increases and then decreases as δ increases from 0 to 1. When $\delta = M_{rs}/(aL_s)$, the amplitude of I_s reaches its maximum. Therefore, δ should satisfy the following condition:

$$\delta = M_{rs}/(aL_s). \tag{23}$$

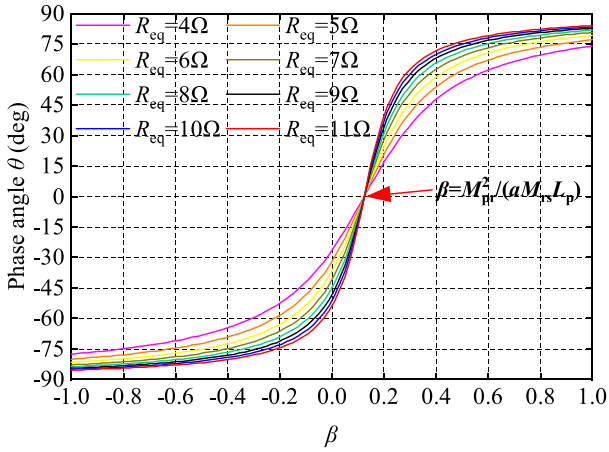

Fig. 8. Variation of phase angle (θ) against β in alignment.

Subsequently, (17) can be further derived as follows:

$$\begin{cases} \dot{I}_f = \frac{\dot{U}_{ac}M_{eq}^2}{a^2L_f^2R_{eq}} + \frac{\dot{U}_{ac}(M_{pr}^2 - a\beta M_{rs}L_p)}{aj\omega M_{rs}L_f^2} \\ \dot{I}_p = \dot{U}_{ac}/(j\omega L_f) \\ \dot{I}_r = \frac{-\dot{U}_{ac}M_{pr}}{aj\omega M_{rs}L_f} - \frac{\dot{U}_{ac}M_{eq}}{a^2L_fR_{eq}} \\ \dot{I}_s = \dot{U}_{ac}M_{eq}/(aL_fR_{eq}). \end{cases} \tag{24}$$

3) Design Transmitting Coil Tuning Ratio β: After the Ix tuning ratio γ and the Rx tuning ratio δ have been determined, we continue to determine the Tx tuning ratio β, which affects the imaginary part of the inverter output current I_f according to (24). The phase angle θ between the output current I_f and the output voltage U_{ac} of the inverter can be expressed as

$$\theta = \arctan\left[\frac{aR_{eq}(a\beta M_{rs}L_p - M_{pr}^2)}{\omega M_{rs}{M_{eq}}^2}\right]\frac{180^\circ}{\pi}. \tag{25}$$

ZVS can ensure that the voltage across the MOSFET switching is close to zero during the switching process, thereby avoiding significant losses caused by the overlap of voltage and current at the of switching process; and it is affected by voltage and current phase angle θ, when $\theta \leq 0$, the ZVS of the inverter can be achieved. According to (25), voltage and current phase angle θ can be adjusted by β.

Fig. 8 shows the variation of the voltage and current phase angle θ against β in alignment. We can conclude that at the moment of alignment, when $\beta = M_{pr}^2/(aM_{rs}L_p)$, $\theta = 0^\circ$, ZVS can be achieved at this time. However, when β gradually increases from $M_{pr}^2/(aM_{rs}L_p)$ to 1, θ gradually increases from 0° to 90°. Generally, in the design process, it is typically required that $0 \leq \beta$. Therefore, to achieve ZVS for the inverter, β should satisfy the condition: $0 \leq \beta \leq M_{pr}^2/(aM_{rs}L_p)$.

Subsequently, according to (25), if M_{eq} is a constant value during the misalignment process, then M_{pr} is the only variable value in this process. Therefore, the variation of θ with misalignment can be expressed as a variation of θ with M_{pr}. Then the relationship between the phase angle θ and variable β with misalignment is shown in Fig. 9, and it can be seen that when $\beta = 0$, the phase angle $\theta \leq 0^\circ$. If $\theta \leq 0^\circ$, the current phase lags behind the voltage phase, allowing the MOSFET to achieve

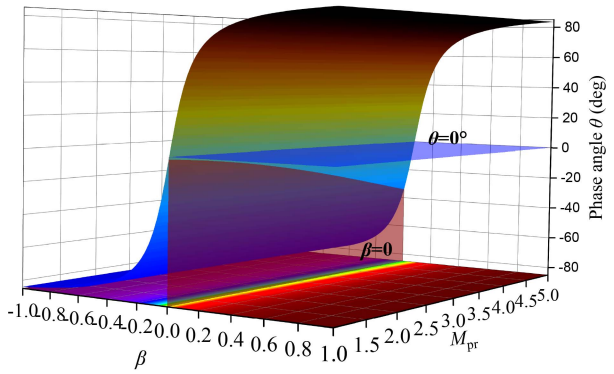

Fig. 9. Variation of phase angle (θ) against β and $M_{\rm pr}$.

zero-voltage turn-ON and enabling the inverter to achieve ZVS. Therefore, to achieve ZVS of inverter, β should be set to zero $\beta = 0$, and (24) is expressed as

$$\begin{cases} \dot{I}_{\rm f} = \dfrac{\dot{U}_{\rm ac} M_{\rm eq}^2}{a^2 L_{\rm f}^2 R_{\rm eq}} + \dfrac{\dot{U}_{\rm ac} M_{\rm pr}^2}{aj\omega M_{\rm rs} L_{\rm f}^2} \\ \dot{I}_{\rm p} = \dot{U}_{\rm ac}/(j\omega L_{\rm f}) \\ \dot{I}_{\rm r} = \dfrac{-\dot{U}_{\rm ac} M_{\rm pr}}{aj\omega M_{\rm rs} L_{\rm f}} - \dfrac{\dot{U}_{\rm ac} M_{\rm eq}}{a^2 L_{\rm f} R_{\rm eq}} \\ \dot{I}_{\rm s} = \dot{U}_{\rm ac} M_{\rm eq}^2/(aL_{\rm f} R_{\rm eq}). \end{cases} \tag{26}$$

According to (26), the intermediate coil current is related to $M_{\rm pr}$, $M_{\rm eq}$, and $M_{\rm rs}$; however, $M_{\rm eq}$ and $M_{\rm rs}$ remain fixed values, while only $M_{\rm pr}$ changes during the misalignment process. Therefore, the intermediate coil current $\dot{I}_{\rm r}$ will vary with $M_{\rm pr}$ during the misalignment process. From (25), the phase between $\dot{U}_{\rm ac}$ and $\dot{I}_{\rm s}$ is in phase. Therefore, the phase difference between $\dot{I}_{\rm r}$ and $\dot{I}_{\rm s}$ can be expressed in terms of the phase difference between $\dot{I}_{\rm r}$ and $\dot{U}_{\rm ac}$. The phase angle φ between the Ix current $\dot{I}_{\rm r}$ and the Rx current $\dot{I}_{\rm s}$ can be expressed as

$$\varphi = \arctan\left(-\frac{aM_{\rm pr}R_{\rm eq}}{\omega M_{\rm rs} M_{\rm eq}}\right)\frac{180^\circ}{\pi}. \tag{27}$$

Fig. 10 shows the variation of phase angle φ with misalignment. From Fig. 10, as $M_{\rm pr}$ decreases during the misalignment, the phase angle φ between the intermediate coil current and voltage of inverter approaches 0 from a negative value.

The output voltage on the ac side of the system described by (6) can be expressed as

$$\dot{U}_{\rm s} = \dot{I}_{\rm s} R_{\rm eq} = \dot{U}_{\rm ac} M_{\rm eq}/(aL_{\rm f}). \tag{28}$$

Let $k = M_{\rm eq}/(aL_{\rm f})$, (28) can be expressed as

$$\dot{U}_{\rm s} = k\dot{U}_{\rm ac}. \tag{29}$$

The output power on the ac side of the system described by (7) can be expressed as

$$P_{\rm out} = |\dot{U}_{\rm s}||\dot{I}_{\rm s}|\cos\theta = \frac{U_{\rm ac}^2 {M_{\rm eq}}^2}{a^2 L_{\rm f}^2 R_{\rm eq}}. \tag{30}$$

According to (29), the output voltage $\dot{U}_{\rm s}$ of the system is independent of the load $R_{\rm eq}$, allowing the system to achieve a constant voltage output. The ratio of $\dot{U}_{\rm s}/\dot{U}_{\rm ac}$ is k, and the system

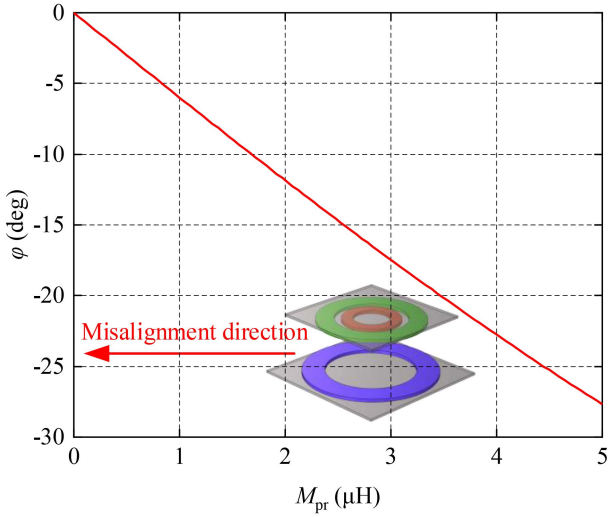

Fig. 10. Variation of phase angle (φ) against $M_{\rm pr}$.

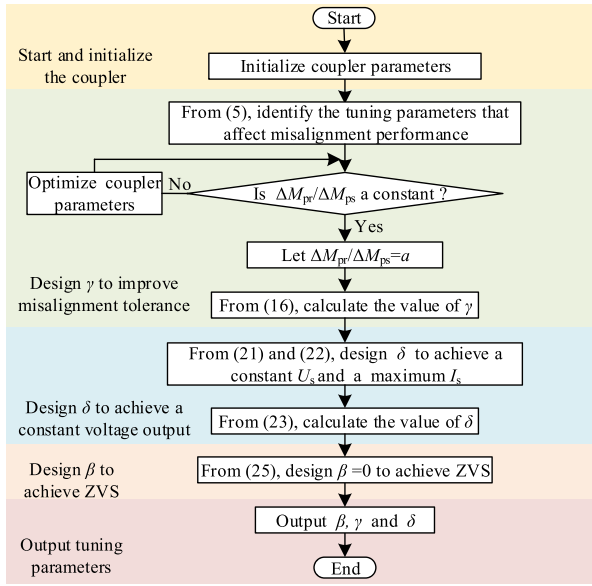

Fig. 11. Design flow of the coils tuning ratio method.

can be considered a transformer with a voltage transformation ratio of k.

To facilitate the design of tuning ratio parameters, the design flow of the coils tuning ratio method is summarized in Fig. 11, which outlines the process for designing the tuning ratios β, γ, and δ to improve misalignment tolerance of the system, achieve constant output voltage and maximum power transfer capacity, and ensure ZVS of the inverter. This design flow simplifies the process of designing the tuning ratios β, γ, and δ, and some remarks on this flowchart are as follows.

1) First, analysis the tuning ratio parameter that affects the system's misalignment tolerance. Then, optimize this parameter to ensure that the system output remains constant and independent of misalignment. In this article, this parameter is γ, and according to (16), let $\gamma = aM_{\rm rs}/L_{\rm r}$.

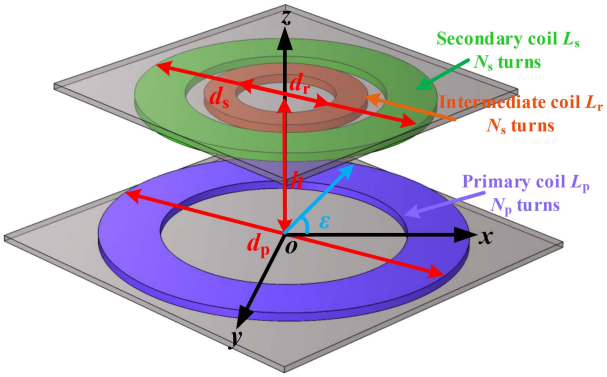

Fig. 12. Definition of coil size and structure.

TABLE II
DEFINITION OF COILS PARAMETERS

Symbol	Definition	Unit
d_p	Diameter of transmitter coil	mm
d_r	Diameter of repeater coil	mm
d_s	Diameter of receiver coil	mm
d	Wire diameter for winding	mm
N_p	Turns of transmitter	/
N_r	Turns of repeater	/
N_s	Turns of receiver	/
h	Distance between transmitter and receiver	mm
ε	Angle between any point on the Tx and the positive direction of x-axis	deg

2) Second, building on the analysis of the first step to improve the system's misalignment tolerance, this step analysis the tuning parameters that affects the system's output voltage and power, then optimizes these parameters to ensure that the output voltage remains independent of the load while maximizing output power. In this article, this parameter is δ, and according to (23), let $\delta = M_{rs}/aL_s$.
3) Finally, based on the analysis of the first and second steps, this step analysis the conditions for achieving ZVS turn-ON of the system inverter. In this article, β affects the switching state of the system inverter. To achieve ZVS throughout the entire misalignment process, β is set to 0.

The system tuning parameters can be calculated simply by the above three steps, making the calculation simple and convenient.

B. Coupler and Magnetic Analysis

1) Coupler Design: In the WPT system, the coils are typically either square or circular. Square coils are symmetric only in the x and y directions of the plane, while circular coils are symmetric throughout the entire plane. To achieve high misalignment tolerance for the system in all directions across the entire plane, the Tx, Ix, and Rx are all designed as circular coils. The structure and dimensions of coils are shown in Fig. 12, and the definition of each parameter is shown in Table II.

The design flow to design a coupler that satisfies (15) is shown in Fig. 13. This flowchart simplifies the process of developing the desired coupler. The flowchart can be decomposed into four steps as follows.

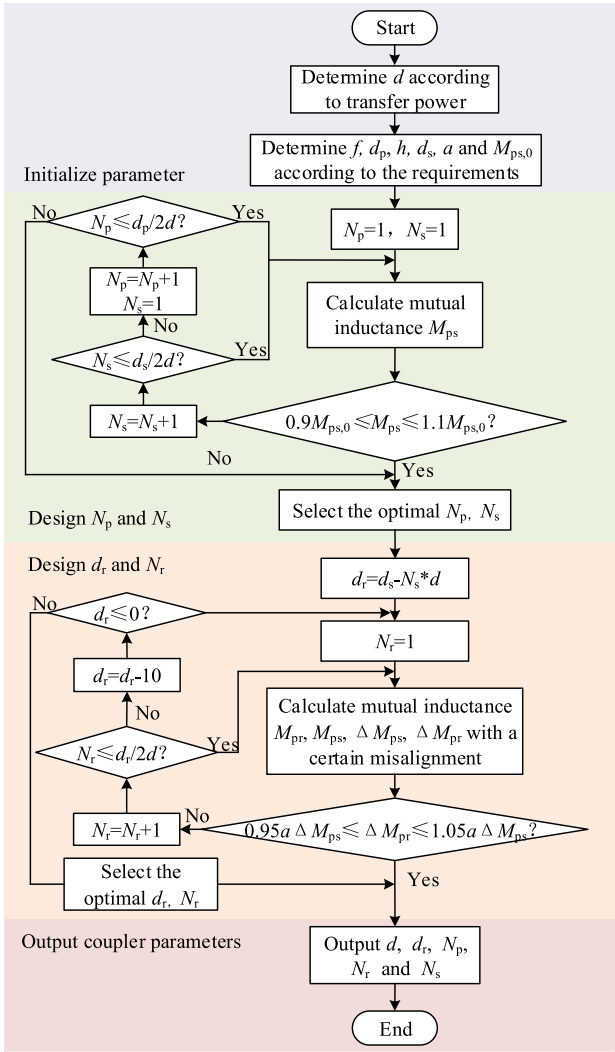

Fig. 13. Design flow of coupling mechanism.

1) First, determine d according to the Tx, Ix and Rx currents. Then, determine f, a, d_p, h, d_s and $M_{ps,0}$ based on practical requirements.
2) Secondbackslas, design parameters of Tx and Rx for N_p and N_s.
3) Third, design parameters of Ix for d_r and N_r.
4) Finally, output the parameters of d_r, N_p, N_r, N_s, and d.

According to the coupler design flow, a coupler that satisfies (15) has been designed. The specific parameters of the coupling mechanism are shown in Table III.

When $a = 1$, (18) is further derived as

$$M_{eq} = M_{pr} - M_{ps}. \tag{31}$$

Fig. 14 shows the COMSOL finite element simulations and actual measurements of L_p, L_r, L_s, and M_{rs} both in alignment and misalignment. It can be seen that the measured values are highly consistent with the simulated values. L_p, L_r, L_s, and M_{rs} remain constant in the presence of misalignment.

Fig. 15 shows the COMSOL finite element simulations and actual measurements of M_{ps}, M_{pr}, and M_{eq} in all planar misalignment directions. There are small errors between simulated

TABLE III
PARAMETER OF DESIGN COUPLING MECHANISM

Parameter	Value	Parameter	Value
f	85 kHz	d_p	150 mm
d_r	140 mm	d_s	250 mm
d	2.8 mm	h	50 mm
N_p	16	N_r	12
N_s	15	a	1
L_p	32.2 μH	L_r	19.6 μH
L_s	77.6 μH	$M_{\mathrm{ps},0}$	9.7 μH
$M_{\mathrm{pr},0}$	5.06 μH	$M_{\mathrm{rs},0}$	12.6 μH

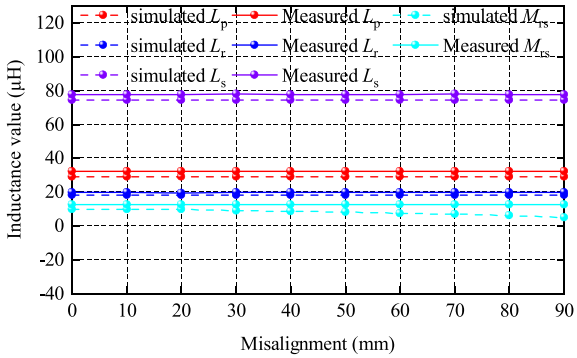

Fig. 14. Simulated and measured of L_p, L_r, L_s, and M_rs with planar misalignment.

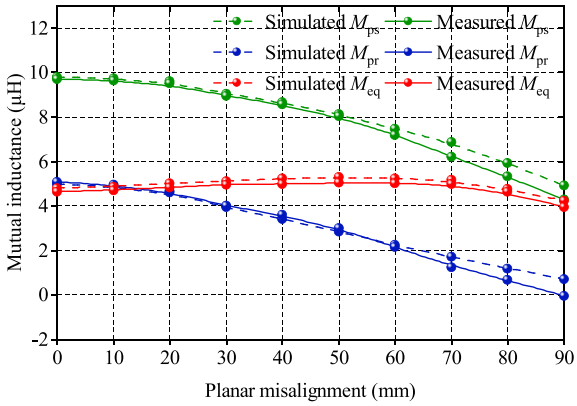

Fig. 15. Simulated and measured of M_ps, M_pr, and M_eq with planar misalignment.

and measured values of M_ps, M_pr and M_eq for the 0–90 mm misalignment range. These errors are acceptable and within practical limits. When the fluctuation of M_eq remains within ± 2 %, the maximum allowable misalignment is 70 mm (46.67% of the diameter of the Tx), while the fluctuation of M_eq remains within ± 3 %, the maximum allowable misalignment is 80 mm (53.3% of the diameter of the Tx).

Fig. 16 shows the COMSOL finite element simulations and actual measurements of M_ps, M_pr, and M_eq in vertical misalignment direction. From Fig. 16, the measured values of M_ps, M_pr, and M_eq are almost identical to the simulated values. When the transfer distance increases gradually from 30–65 mm, M_eq is approximately a constant value, and the fluctuation of M_eq remains within $\pm$ 5%. When the transfer distance increases gradually from 30 to 70 mm, the fluctuation of M_eq remains

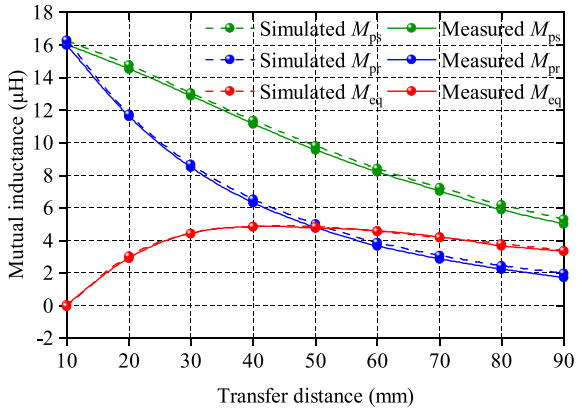

Fig. 16. Simulated and measured of M_ps, M_pr and M_eq with vertical misalignment.

within $\pm$ 8%. In conclusion, M_eq remains constant in all planar directions and within 30–65 mm transfer distance in the vertical direction.

Therefore, based on the above analysis, the parameter M_eq remains approximately constant within the horizontal misalignment range of 0–80 mm and the vertical misalignment range of 30–65 mm. From Fig. (15) and (16), a is also approximately constant within the above misalignment range.

2) Magnetic Analysis: To analyze the physical mechanism of the proposed method in this article, a magnetic field analysis is conducted. The magnetic induction components in the x, y, and z directions at point $P(x_0, y_0, z_0)$ in space generated by the Tx can be expressed as $\boldsymbol{B}_\mathrm{x}$, $\boldsymbol{B}_\mathrm{y}$, and $\boldsymbol{B}_\mathrm{z}$

$$\begin{cases} B_\mathrm{x} = \frac{\mu_0 N_\mathrm{p} I_\mathrm{p}}{4\pi} \int_0^{2\pi} \frac{z_0}{r^3} y' \mathrm{d}\varepsilon \\ B_\mathrm{y} = -\frac{\mu_0 N_\mathrm{p} I_\mathrm{p}}{4\pi} \int_0^{2\pi} \frac{z_0}{r^3} x' \mathrm{d}\varepsilon \\ B_\mathrm{z} = \frac{\mu_0 N_\mathrm{p} I_\mathrm{p}}{4\pi} \int_0^{2\pi} \frac{(y_0 - y)x' - (x_0 - x)y'}{r^3} \mathrm{d}\varepsilon \end{cases} \tag{32}$$

where r represents the distance from any point on the Tx to the point $P(x_0, y_0, z_0)$ in space, and x, y, ε represent the coordinates of a point on the Tx

$$r = \sqrt{(x_0 - x)^2 + (y_0 - y)^2 + (z_0 - z)^2}$$

$$\begin{cases} x = \frac{d_p}{2} \cos(\varepsilon) \\ y = \frac{d_p}{2} \sin(\varepsilon) \\ \varepsilon \in [0, 2\pi]. \end{cases}$$

According to the principle of magnetic field vector superposition, the resultant magnetic flux density $\boldsymbol{B}$ generated by the Tx at any point $P(x_0, y_0, z_0)$ in space can be expressed as

$$\boldsymbol{B} = \begin{bmatrix} B_\mathrm{x} \\ B_\mathrm{y} \\ B_\mathrm{z} \end{bmatrix}. \tag{33}$$

The magnetic flux through the Ix and Rx can be expressed as

$$\begin{cases} \Phi_\mathrm{r} = N_\mathrm{r} \int_{S_\mathrm{r}} \boldsymbol{B} \cdot \mathrm{d}\boldsymbol{A}_\mathrm{r} \\ \Phi_\mathrm{s} = N_\mathrm{s} \int_{S_\mathrm{s}} \boldsymbol{B} \cdot \mathrm{d}\boldsymbol{A}_\mathrm{s}. \end{cases} \tag{34}$$

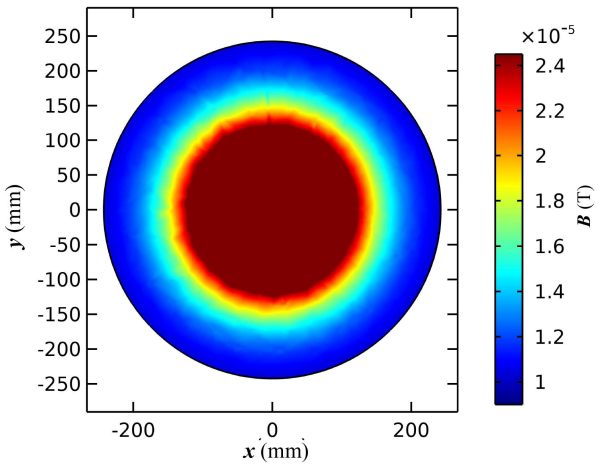

Fig. 17. Magnetic flux density distribution.

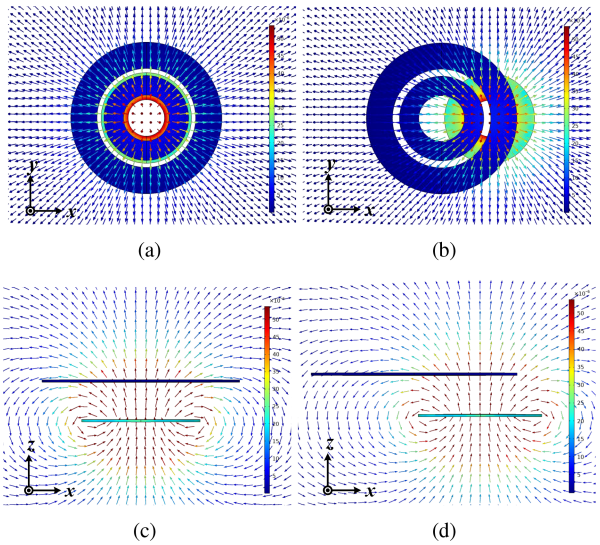

Fig. 18. Magnetic field distribution. (a) Top view in a well-alignment. (b) Top view with 80 mm misalignment. (c) Front view with in a well-alignment. (d) Front view with 80 mm misalignment.

The mutual inductance $M_{\rm ps}$ and $M_{\rm pr}$ can be expressed as

$$\begin{cases} M_{\rm ps} = \frac{\Phi_{\rm s}}{I_{\rm p}} \\ M_{\rm pr} = \frac{\Phi_{\rm r}}{I_{\rm p}}. \end{cases} \tag{35}$$

When the misalignment occurs, $\Delta M_{\rm ps}$ and $\Delta M_{\rm pr}$ can be expressed as

$$\begin{cases} \Delta M_{\rm ps} = \frac{\Phi_{\rm s,0} - \Phi_{\rm s}}{I_{\rm p}} \\ \Delta M_{\rm pr} = \frac{\Phi_{\rm r,0} - \Phi_{\rm r}}{I_{\rm p}}. \end{cases} \tag{36}$$

The distribution of the magnetic flux density $\boldsymbol{B}$ observed on the plane at $z = 50$ mm is shown in Fig. 17.

The magnetic field distribution both in a well-aligned condition and with 80 mm misalignment is shown in Fig. 18(a), (b), (c), and (d), obtained using COMSOL finite element simulation software. In Fig. 18(a) and (c), the Ix and Rx are fully coupled with Tx. In Fig. 18(b) and (d), only the edges of the Ix and the Rx are coupled with the Tx. As the misalignment increases, the coupling area between the Ix and the Tx, as well as between the Rx and the Tx, becomes progressively smaller. Consequently, both $M_{\rm ps}$ and $M_{\rm pr}$ will decrease simultaneously with misalignment. The prototype and size of the designed coupler is shown in Fig. 19, which shows that the diameter of the Tx, Ix, and Rx are 150 mm, 140 mm, and 250 mm, respectively. The transfer distance h is 50 mm.

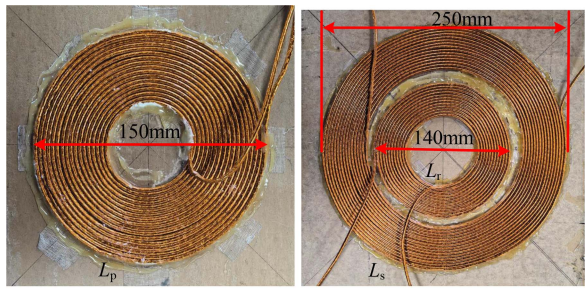

Fig. 19. Prototype of coupling mechanism. (a) Tx. (b) Ix and Rx.

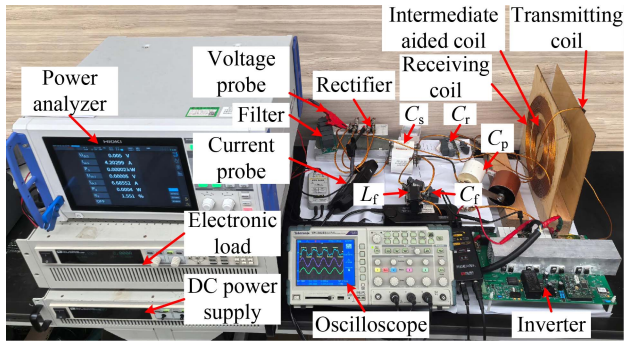

Fig. 20. 500 W experimental prototype.

IV. Experimental Results

A. Experiment and Output Performance

To validate the effectiveness of the proposed SIA WPT system, a 500-W experimental prototype has been constructed, as shown in Fig. 20, and the system parameters are listed in Table IV. To measure the input/output voltage, current, power, and system efficiency, a power analyzer (Model: HIOKI PW8001) is employed in this article.

Fig. 21 shows the experimental waveforms with $R_{\rm L} = 3.8\,\Omega$ for the inverter output voltage $U_{\rm ac}$ and current $I_{\rm f}$, the rectifier input voltage $U_{\rm s}$ and current $I_{\rm s}$, as well as the intermediate coil current $I_{\rm r}$, all in perfect alignment. In Fig. 21, the inverter output voltage is set to 100 V/div and rectifier input voltage is set to 50 V/div, while the inverter output current, the intermediate coil current and the rectifier input voltage and current are set to 15 A/div, 30 A/div, and 30 A/div. From Fig. 21(a), the inverter output current $I_{\rm f}$ lags the inverter output voltage $U_{\rm ac}$ by a certain phase angle, indicating that the inverter achieves ZVS in a well-aligned. From Fig. 21(b), the intermediate coil current $I_{\rm r}$

TABLE IV
SYSTEM PARAMETER

Parameter	Value	Parameter	Value
f	85kHz	U_{dc}	100V
L_f	10 μH	C_f	350.6nF
L_p	32.2 μH	C_p	159.4nF
L_r	19.6 μH	C_r	493.9nF
L_s	77.6 μH	C_s	53.86nF
U_o	43V	$M_{ps,0}$	9.7 μH
$M_{pr,0}$	5.06 μH	$M_{rs,0}$	12.6 μH
α	0	β	0
γ	0.64	δ	0.16
k	0.46		

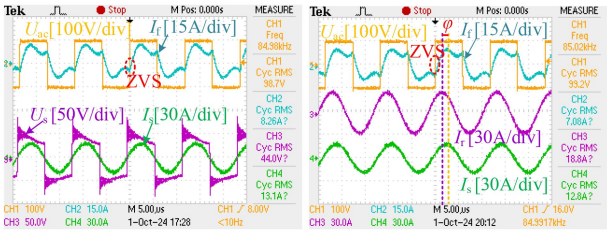

(a) (b)

Fig. 21. Experimental waveforms in a well-alignment when $R_L = 3.8\ \Omega$. (a) the waveforms of U_{ac}, I_f, U_s, and I_s. (b) The waveforms of U_{ac}, I_f, I_r, and I_s.

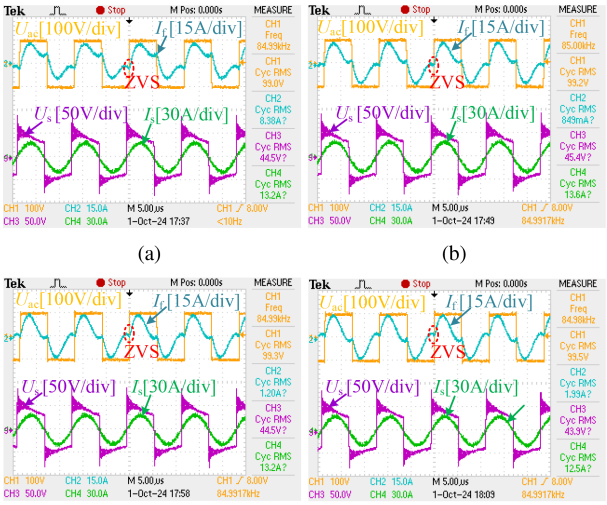

(a) (b)

(c) (d)

Fig. 22. Experimental waveforms of U_{ac}, I_f, U_s, and I_s with planar misalignment when $R_L = 3.8\ \Omega$. (a) With 20 mm planar misalignment. (b) With 40 mm planar misalignment. (c) With 60 mm planar misalignment. (d) With 80 mm planar misalignment.

leads the inverter output voltage U_{ac} by φ, the correctness of theoretical analysis has been verified.

The experimental waveforms with $R_L = 3.8\,\Omega$ for the inverter output voltage U_{ac} and current I_f, while the rectifier input voltage U_s and current I_s for 20 mm, 40 mm, 60 mm, and 80 mm planar misalignments are shown in Fig. 22. As can be seen from

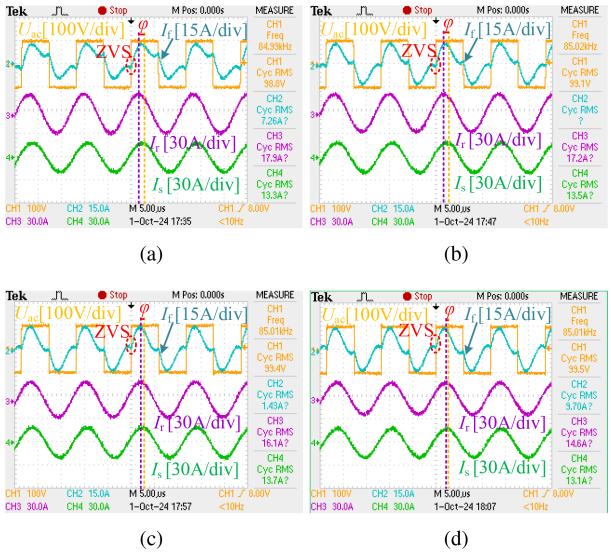

(a) (b)

(c) (d)

Fig. 23. Experimental waveforms of U_{ac}, I_f, I_r, and I_s with planar misalignment when $R_L = 3.8\ \Omega$. (a) With 20 mm planar misalignment. (b) With 40 mm planar misalignment. (c) With 60 mm planar misalignment. (d) With 80 mm planar misalignment.

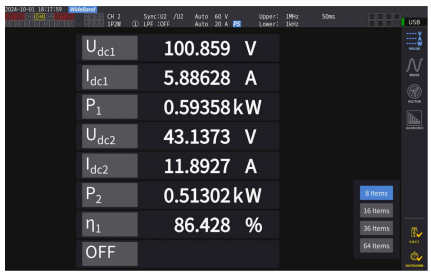

Fig. 24. System electrical parameters in a perfect-alignment.

Fig. 22(a), (b), (c), and (d), the inverter output current I_f lags the inverter output voltage U_{ac} by a certain phase angle, or the inverter output current I_f and the inverter output voltage U_{ac} turn ON simultaneously, indicating that the inverter achieves ZVS for all misalignments.

Fig. 23 shows the experimental waveforms with $R_L = 3.8\,\Omega$ for the inverter output voltage U_{ac} and current I_f, the intermediate coil current I_r, and the rectifier input current I_s for 20 mm, 40 mm, 60 mm, and 80 mm planar misalignments. As can be seen from Fig. 23(a), (b), (c), and (d), the phase angle φ between the intermediate coil current I_r and the inverter output voltage U_{ac} gradually decreases as the misalignment distance increases, confirming the correctness of the theoretical analysis.

The electrical parameters at the dc side and the system's dc–dc efficiency at the well-aligned is shown in Fig. 24, where U_{dc1}, I_{dc1}, and P_1 represent the system's input dc voltage, dc current, and input power, while U_{dc2}, I_{dc2}, and P_2 represent the system's dc output voltage, dc current, and output power. η_1 is the system's dc–dc efficiency. It can be seen that the system's dc input voltage and current are 100.86V and 5.89A, the dc output voltage and

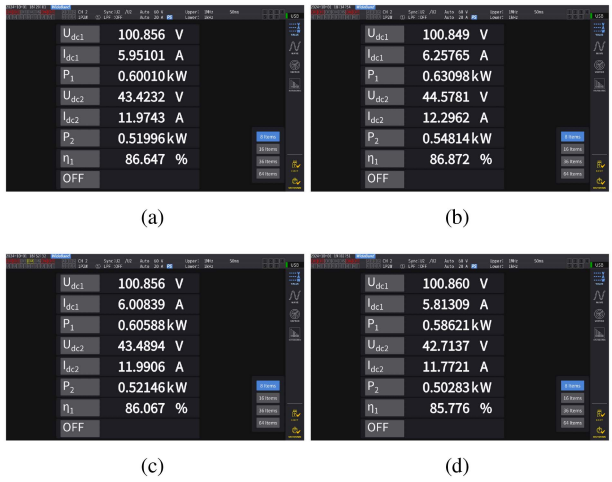

Fig. 25. System electrical parameters of U_{dc}, I_{dc}, U_{o}, and I_{o} with planar misalignment when $R_{\mathrm{L}} = 3.8\,\Omega$. (a) With 20 mm planar misalignment. (b) With 40 mm planar misalignment. (c) With 60 mm planar misalignment. (d) With 80 mm planar misalignment.

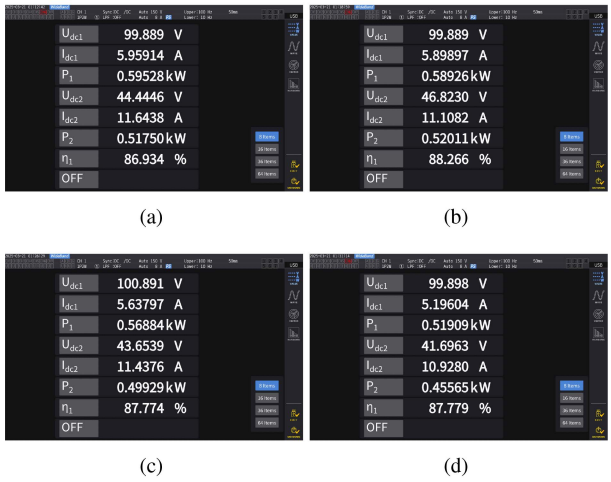

Fig. 26. System electrical parameters of U_{dc}, I_{dc}, U_{o}, and I_{o} with vertical transfer distance when $R_{\mathrm{L}} = 3.8\,\Omega$. (a) With 30 mm vertical transfer distance. (b) With 40 mm vertical transfer distance. (c) With 60 mm vertical transfer distance. (d) With 70 mm vertical transfer distance.

output current are 43.14 V and 11.89 A, while the dc–dc transfer efficiency is 86.43%.

When load resistance is $R_{\mathrm{L}} = 3.8\,\Omega$, the electrical parameters at the dc side and the system's dc–dc efficiency for 20 mm, 40 mm, 60 mm, and 80 mm planar misalignments are shown in Fig. 25. As can be seen from Fig. 25(a), (b), (c), and (d), the system's dc input voltage ranges between 100.85V and 100.86V, while the system's dc output voltage ranges between 42.71 V and 44.58 V, and the system's transfer efficiency ranges between 85.78% and 86.87%.

The output parameters of the SIA WPT system are shown in Fig. 26 when vertical misalignment occurs with $R_{\mathrm{L}} = 3.8\,\Omega$. Fig. 26(a), (b), (c), and (d) display the input/output voltage, current, power, and efficiency at vertical transfer distances of 30 mm, 40 mm, 60 mm, and 70 mm, respectively. Within the

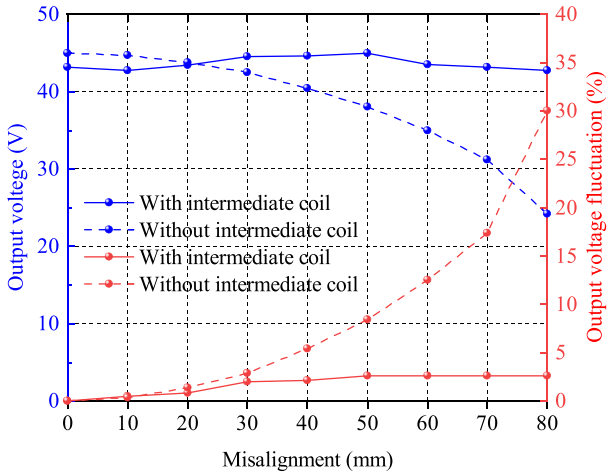

Fig. 27. Output voltage and output voltage fluctuation with planar misalignment.

transfer distance range of 30–70 mm, the system's dc–dc efficiency remains between 86.43% and 88.27%, while the output voltage stays between 41.7 V and 46.82 V.

To verify the effectiveness and feasibility of the SIA WPT system and the proposed tuning method in this article, the misalignment tolerance performance of both the traditional two-coil system and the SIA WPT system are analyzed under the same conditions, including coil size, input voltage, output voltage, transfer distance, and transfer efficiency.

Fig. 27 shows the output voltage and output voltage fluctuation with planar misalignment. The output voltage fluctuation ratio is defined as follows:

$$\lambda = \frac{U_{\mathrm{o\_max}} - U_{\mathrm{o\_min}}}{U_{\mathrm{o\_max}} + U_{\mathrm{o\_min}}} \times 100\% \tag{37}$$

where $U_{\mathrm{o\_max}}$ and $U_{\mathrm{o\_min}}$ are the maximum output voltage and the minimum output voltage of system with misalignment.

In well-aligned, the output voltage of the SIA WPT system is 43.14 V. With a 50 mm planar misalignment, the output voltage increases to a maximum of 45 V, with an output voltage fluctuation ratio $\lambda = 2.58\%$. At 80 mm planar misalignment (53.3%) and when the load resistance is $R_{\mathrm{L}} = 3.8\,\Omega$, the output voltage of the SIA WPT system decreases to a minimum of 42.71V, with an output voltage fluctuation ratio $\lambda = 2.61\%$. Moreover, in the perfect alignment case, the output voltage of the traditional two-coil system is 45 V. With a 25 mm planar misalignment and $R_{\mathrm{L}} = 3.8\,\Omega$, the output voltage decreases to 42.7 V, and the traditional two-coil system output voltage fluctuation is $\lambda = 2.62\%$. With a 80-mm planar misalignment, the output voltage of the traditional two-coil system drops to 27.71V with the fluctuation of output voltage $\lambda = 23.78\%$. Compared to the traditional two-coil system, the planar misalignment tolerance is increased by 55 mm (36.7% of the transmitter diameter) indicating that the SIA WPT system significantly improves the planar misalignment tolerance.

Fig. 28 shows the output power and efficiency of the SIA WPT system and the traditional two-coil system with planar misalignment when the load resistance is $R_{\mathrm{L}} = 3.8\,\Omega$. In well-alignment,

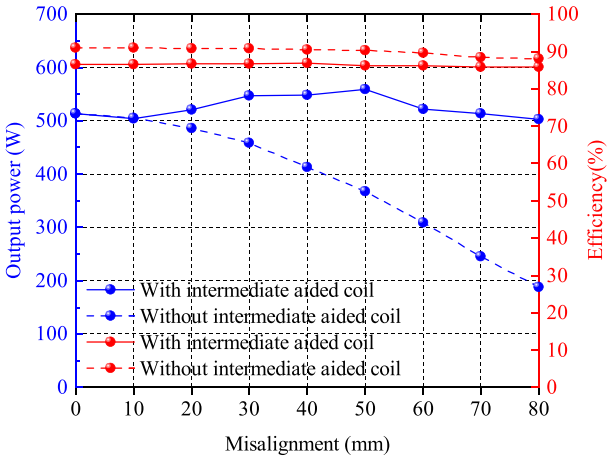

Fig. 28. Output power and efficiency against planar misalignment.

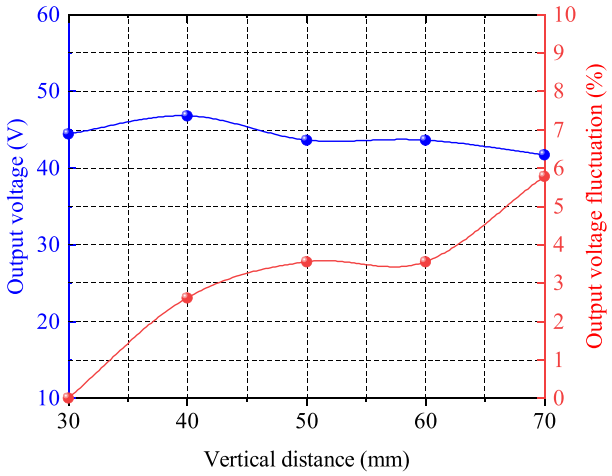

Fig. 29. Output voltage and fluctuation ratio of the SIA WPT system against vertical distance.

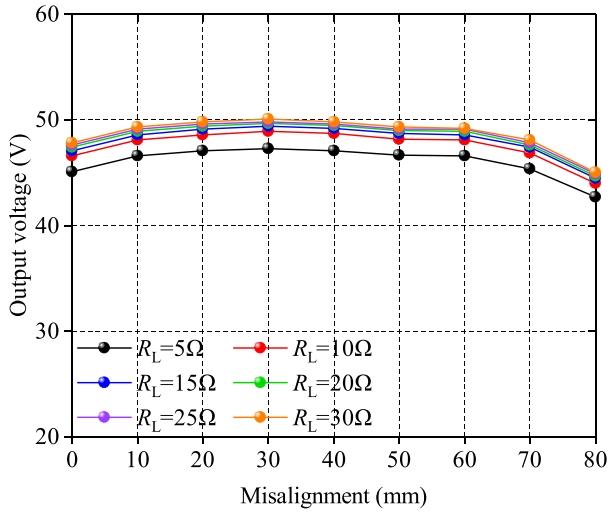

Fig. 30. Output voltage with planar misalignment and load.

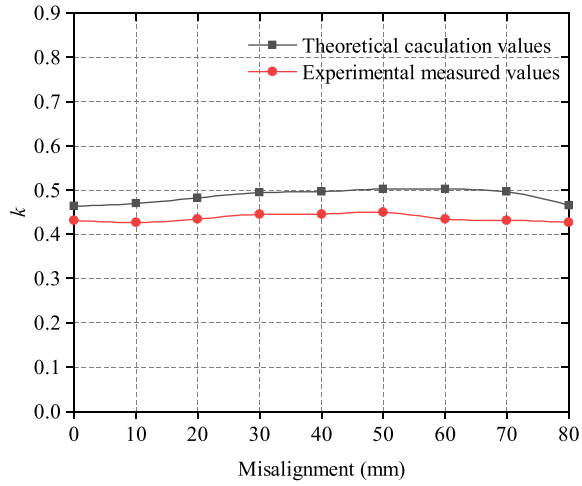

Fig. 31. Comparison between theoretical and measured values of k.

the output power of the SIA WPT system is 513 W, and the dc–dc efficiency is 86.43%. Meanwhile, the output power of the two-coil system is 513 W, and the dc–dc efficiency is 90.95%. With a 50-mm planar misalignment, the output power of the SIA WPT system increases to a maximum of 558.94 W, and the dc–dc efficiency is 86.14%. With a 80 mm planar misalignment, the output power of the SIA WPT system is 502.83 W, and the dc–dc efficiency is 85.78%. The output power of the traditional two-coil system decreases gradually with increasing planar misalignment. With a 30 mm planar misalignment, the output power of the traditional two-coil system is 477 W, and the dc–dc efficiency is 90.68%. With a 80-mm planar misalignment, the output power of the traditional two-coil system is 187.4 W, and the dc–dc efficiency is 88.02%. The difference in efficiency between the SIA WPT system and the traditional two-coil system is 2.24%.

Fig. 29 shows the output voltage and output voltage fluctuation ratio of the SIA WPT system versus vertical misalignment. When the vertical transfer distance is 40 mm, the system's output voltage reaches a maximum of 46.82 V, while at a distance of 70 mm, the voltage drops to a minimum of 41.7 V. The highest fluctuation occurs at a vertical transfer distance of 70 mm, with a fluctuation ratio of 5.78%. However, within the transfer range of 30–65 mm (70% of transfer distance), the system's output voltage fluctuations remain within 5%. Therefore, the SIA WPT system proposed in this article yields a high tolerance to vertical misalignment.

Fig. 30 shows the output voltage of the SIA WPT system versus planar misalignment and load resistance R_L from 5 Ω to 30 Ω . With a 80 mm planar misalignment and load resistances R_L ranging from 5 Ω to 30 Ω, the output voltage fluctuation is $\lambda = 2.62\%$. Over a planar misalignment range of 0–80 mm and the load from 5 Ω to 30 Ω, the output voltage fluctuation of SIA WPT system is less than 2.7 V, indicating that the system can maintain a constant voltage output.

Fig. 31 shows the theoretical and measured values of k against planar misalignment. Due to the losses in the electronic components during the experiment, the experimental value of k is slightly smaller than the theoretical calculated value. However,

TABLE V
COMPARISON WITH PREVIOUSLY PUBLISHED WORKS

Ref.	Misalignment Directions	Planar Misalignment Percentage (%)	Z-axis misalignment Percentage (%)	Load-independent Output	Output Fluctuation (%)
[17]	Only axial direction	X-axis: 40% Y-axis: 40%	No data	CC	5%
[18]	Only axial direction	X-axis: 43% Y-axis: 43%	No data	CV	5%
[21]	Only axial direction	X-axis: No Y-axis: 33.4%	44.4%	CC	6.2%
[24]	Only axial direction	X-axis: 15.5% Y-axis: 40.9%	16.7%	CP	5%
[28]	Only axial direction	X-axis: 50% Y-axis: 11.1%	46.7%	CC	5%
This Article	**The whole plane and Z-axis**	**Whole plane: 53.3%**	**70%**	**CV**	**planar: 3% vertical: 5%**

during the misalignment process, the variation trend of the measured and the theoretical values remains consistent, proving that the system can be considered as a transformer with a voltage transformation ratio of k.

B. Comparison With Existing Research

The comparison results between the SIA WPT system and previously published works are shown in Table V. This table highlights several key advantages and contributions of the presented work. The comparisons in this article are based solely on the data explicitly reported in the reference articles; any data not provided are assumed to be unavailable. Compared with [17], the proposed SIA WPT system improves misalignment range and accommodates additional misalignment directions.

Compared with [18], a three-coil system structure that employs square coils is proposed in [18]. By designing the coupler to satisfy the condition $\Delta M_{\mathrm{PS}} = \Delta M_{\mathrm{TS}}$ during misalignment, the system significantly improves its misalignment tolerance along both the x-axis and y-axis. If circular coils are further adopted in this system, it is expected to enhance the misalignment tolerance in all directions within the plane. However, this aspect was not discussed in [18]. The system is suitable wireless charging for electric vehicles. However, in certain specific applications–such as automated guided vehicle requiring the transmitting and receiving coils to have identical dimensions–designing the coupler to satisfy the condition $\Delta M_{\mathrm{PS}} = \Delta M_{\mathrm{TS}}$ can lead to a significant reduction in misalignment tolerance. In such cases, further designing the coupler to satisfy the condition $\Delta M_{\mathrm{PS}} = a\Delta M_{\mathrm{TS}}$ can effectively enhance the system's misalignment tolerance. The SIA WPT system proposed in this article effectively overcomes the limitations of the method presented in [18], improving misalignment tolerance—particularly in application scenarios where the transmitting and receiving coils are required to have identical dimensions.

Compared with [21], the proposed SIA WPT system improves misalignment range and accommodates additional misalignment directions. Meanwhile, the coupling mechanism and compensation topology are simpler. Compared with [24], the proposed SIA WPT system improves misalignment range, and the topology structure is simpler. Compared with [28], the proposed SIA WPT system increases the misalignment range and reduces the size of the coupler. To sum up, compared with previously published works, the method proposed in this article improves the system's misalignment tolerance in any lateral direction and vertical direction under planar alignment, and reduces the fluctuation range of the output voltage during the misalignment process. The system tuning parameter design is simple, with only the coupler parameters needing to be provided to calculate the tuning parameters.

V. CONCLUSION

This article has proposed an SIA WPT system with a constant voltage output, introduced a tuning method to enhance the system's planar and vertical misalignment tolerance, and achieve ZVS of the inverter. In this system, the Ix is located at the receiver and wound in the same direction as the Rx to improve the misalignment tolerance, and a tuning method for each coil is proposed. A constant voltage output and high misalignment tolerance are achieved by adjusting the tuning ratio γ of the Ix. Additionally, The system's output current I_{s} can be maximized while the output voltage U_{s} remains independent of the load, thereby achieving both maximum power transfer and constant voltage output by adjusting the tuning ratio δ of the Rx. ZVS of the inverter is achieved by adjusting the tuning ratio β of the Tx. Then, a method for designing the coupling mechanism is proposed based on the system's requirements. Finally, a 500 W experimental prototype has been built to validate the feasibility of the proposed SIA WPT system and the tuning method. The experimental results show that within an 80 mm planar misalignment range (53.3% of the primary coil diameter), the output voltage fluctuation of the SIA WPT system is within 3%, and the peak dc–dc efficiency is 86.87%. In the vertical transmission distance range of 30–65 mm (70% of the normal transfer distance), the output voltage fluctuation is within 5%, with a peak dc–dc efficiency of 88.26%.

REFERENCES

[1] Z. Zhang, H. Pang, A. Georgiadis, and C. Cecati, "Wireless power transfer—An overview," *IEEE Trans. Ind. Electron.*, vol. 66, no. 2, pp. 1044–1058, Feb. 2019.

[2] Y. Fan, Y. Sun, X. Dai, Z. Zuo, and A. You, "Simultaneous wireless power transfer and full-duplex communication with a single coupling interface," *IEEE Trans. Power Electron.*, vol. 36, no. 6, pp. 6313–6322, Jun. 2021.

[3] T. Feng, Z. Zuo, Y. Sun, X. Dai, X. Wu, and L. Zhu, "A reticulated planar transmitter using a three-dimensional rotating magnetic field for free-positioning omnidirectional wireless power transfer," *IEEE Trans. Power Electron.*, vol. 37, no. 8, pp. 9999–10015, Aug. 2022.
[4] T. Li et al., "Design and optimization of a perfectly symmetric planar spiral receiving coil with Low E-field exposure for large-space WPT," *IEEE J. Emerg. Sel. Top. Power Electron.*, early access, Oct., 1, 2024, doi: 10.1109/JESTPE.2024.3471657.
[5] K. Song et al., "A rotation-lightweight wireless power transfer system for solar wing driving," *IEEE Trans. Power Electron.*, vol. 34, no. 9, pp. 8816–8830, Sep. 2019.
[6] Y. Li et al., "Analysis, design, and experimental verification of a mixed high-order compensations-based WPT system with constant current outputs for driving multi string LEDs," *IEEE Trans. Ind. Electron.*, vol. 67, no. 1, pp. 203–213, Jan. 2020.
[7] Y. Fan, Y. Sun, X. Dai, Z. Zuo, and A. You, "Simultaneous wireless power transfer and full-duplex communication with a single coupling interface," *IEEE Trans. Power Electron.*, vol. 36, no. 6, pp. 6313–6322, Jun. 2021.
[8] X. Hou, Y. Su, Z. Zuo, X. Dai, and Y. Fei, "A novel analysis method based on quadratic eigenvalue problem for multirelay magnetic coupling wireless power transfer," *IEEE Trans. Power Electron.*, vol. 36, no. 9, pp. 9907–9917, Sep. 2021.
[9] N. Kang, Y. Shao, M. Liu, and C. Ma, "Analysis and implementation of 3D magnetic field shaping via a 2D planar transmitting coil array," *IEEE Trans. Power Electron.*, vol. 37, no. 1, pp. 1172–1184, Jan. 2022.
[10] H. Hu, H. Hu, F. Chen, X. Dai, and Y. Sun, "Efficiency improvement strategy based on frequency reduction with constant current characteristic for underwater wireless power transfer systems," *IEEE Trans. Power Electron.*, vol. 40, no. 9, pp. 14038–14049, Sep. 2025.
[11] Z. Deng et al., "Design of a 60-kW EV dynamic wireless power transfer system with dual transmitters and dual receivers," *IEEE Trans. Emerg. Sel. Topics Power Electron.*, vol. 12, no. 1, pp. 316–327, Feb. 2024.
[12] Z. Deng et al., "A method based on vector-summing of reduce output power fluctuation for EV-DWPT system with the passive LC network," *IEEE Trans. Transport. Electrific.*, vol. 11, no. 1, pp. 2133–2145, Feb. 2025.
[13] M. Budhia, J. T. Boys, G. A. Covic, and C. Y. Huang, "Development of a single-sided flux magnetic coupler for electric vehicle IPT charging systems," *IEEE Trans. Ind. Electron.*, vol. 60, no. 1, pp. 318–328, Jan. 2013.
[14] A. Zaheer, G. A. Covic, and D. Kacprzak, "A bipolar pad in a 10-kHz 300-W distributed IPT system for AGV applications," *IEEE Trans. Ind. Electron.*, vol. 61, no. 7, pp. 3288–3301, Jul. 2014.
[15] A. Zaheer, D. Kacprzak, and G. A. Covic, "A bipolar receiver pad in a lumped IPT system for electric vehicle charging applications," in *Proc. IEEE Energy Convers. Congr. Expo. (ECCE)*, Raleigh, NC, USA, 2012, pp. 283–290.
[16] Y. Nagatsuka, N. Ehara, and Y. Kaneko, "Compact contactless power transfer system for electric vehicles," in *Proc. Int. Power Electron. Conf. - ECCE ASIA -*, Sapporo, Japan, 2010, pp. 807–813.
[17] G. Yang, S. Dong, C. Zhu, R. Lu, G. Wei, and K. Song, "Design of a high lateral misalignment tolerance magnetic coupler for wireless power transfer systems," in *Proc. IEEE PELS Workshop Emerg. Technol.: Wireless Power Transfer (WoW)*, Chongqing, China, 2017, pp. 34–39.
[18] Y. Chen, R. Mai, Y. Zhang, M. Li, and Z. He, "Improving misalignment tolerance for IPT system using a third-coil," *IEEE Trans. Power Electron.*, vol. 34, no. 4, pp. 3009–3013, Apr. 2019.
[19] J. Mai, Y. Wang, Y. Yao, M. Sun, and D. Xu, "High-misalignment-Tolerant IPT systems with solenoid and double d pads," *IEEE Trans. Ind. Electron.*, vol. 69, no. 4, pp. 3527–3535, Apr. 2022.
[20] Y. Yao, S. Gao, J. Mai, X. Liu, X. Zhang, and D. Xu, "A novel misalignment tolerant magnetic coupler for electric vehicle wireless charging," *IEEE J. Emerg. Sel. Topics Ind. Electron.*, vol. 3, no. 2, pp. 219–229, Apr. 2022.
[21] X. Li et al., "A dual-coupled Double-LCC system with the capability of misalignment tolerance improvement for wireless charging substation inspection robots," *IEEE Trans. Power Electron.*, vol. 39, no. 6, pp. 6624–6629, Jun. 2024.
[22] F. Hao, A. Dayerizadeh, and S. Lukic, "A coupling-insensitive X-type IPT system for high position tolerance," *IEEE Trans. Ind. Electron.*, vol. 68, no. 8, pp. 6917–6926, Aug. 2021.
[23] H. Jia, Q. Chen, Z. Zhang, S.-C. Wong, and C. K. Tse, "Analysis of output current characteristics for higher order primary compensation in inductive power transfer systems," in *IEEE Trans. Power Electron.*, vol. 33, no. 8, pp. 6807–6821, Aug. 2018.
[24] Z. Lei, D. Thrimawithana, and U. Madawala, "Hybrid bidirectional wireless EV charging system tolerant to pad misalignment," *IEEE Trans. Ind. Electron.*, vol. 64, no. 9, pp. 7079–7086, Sep. 2017.
[25] L. Zhao, D. J. Thrimawithana, U. K. Madawala, A. P. Hu, and C. C. Mi, "A misalignment-tolerant series-hybrid wireless EV charging system with integrated magnetics," *IEEE Trans. Power Electron.*, vol. 34, no. 2, pp. 1276–1285, Feb. 2019.
[26] X. Qu, Y. Yao, D. Wang, S.-C. Wong, and C. K. Tse, "A family of hybrid IPT topologies with near load-independent output and high tolerance to pad misalignment," *IEEE Trans. Power Electron.*, vol. 35, no. 7, pp. 6867–6877, Jul. 2020.
[27] Y. Liu, U. K. Madawala, R. Mai, and Z. He, "An optimal multivariable control strategy for inductive power transfer systems to improve efficiency," *IEEE Trans. Power Electron.*, vol. 35, no. 9, pp. 8998–9010, Sep. 2020.
[28] E. Gati, G. Kampitsis, and S. Manias, "Variable frequency controller for inductive power transfer in dynamic conditions," in *IEEE Trans. Power Electron.*, vol. 32, no. 2, pp. 1684–1696, Feb. 2017.
[29] R. Mai, B. Yang, Y. Chen, N. Yang, Z. He, and S. Gao, "A misalignment tolerant IPT system with intermediate coils for constant-current output," *IEEE Trans. Power Electron.*, vol. 34, no. 8, pp. 7151–7155, Aug. 2019.
[30] S.-J. Huang, T.-S. Lee, Y.-M. Yang, and J.-Y. Chen, "Intermediate coil-aided wireless charging via interactive power transmitting with misalignment-tolerating considerations," *IEEE Trans. Ind. Electron.*, vol. 69, no. 10, pp. 9972–9983, Oct. 2022.

Yingjie Li received the B.E. degree in automation from the Department of Automation, Shanxi University, Shanxi, China, in 2020. He is currently working toward the Ph.D. degree in control science and engineering with the College of Automation, Chongqing University, Chongqing, China.

His current research interests include wireless power transfer and improving misalignment tolerance of wireless power transfer system.

Zhiping Zuo received the B.E. degree in electrical engineering from the College of Electrical and Electronic Engineering, Huazhong University of Science and Technology, Wuhan, China, in 2012, and the Ph.D. degree in electrical engineering from the College of Electrical Engineering, Chongqing University, Chongqing, China, in 2017.

He is currently an Associate Professor with the College of Automation, Chongqing University. His current research interests include fabrication of anticing materials application on insulators and wireless power transfer.

Fengwei Chen was born in Chongqing, China. He received the B.Eng. degree in automation and the M.Eng. degree in control theory and control engineering from Wuhan University, Wuhan, China, in 2009 and 2011, respectively, and the Ph.D. degree in automatic control from the Université de Lorraine, Nancy, France, in 2014.

From 2015 to 2016, he was a Lecturer with the Dalian University of Technology, Dalian, China. From 2017 to 2020, he was an Associate Researcher with Wuhan University. Since 2021, he has been with Chongqing University, Chongqing, where he is currently an Associate Professor. His research interests include system identification and parameter estimation, with applications to wireless power transfer.

Chunsen Tang received the B.S. and Ph.D. degrees in control theory and control engineering from the College of Automation, Chongqing University, Chongqing, China, in 2004 and 2009, respectively.

In 2008, he joined the Department of Electrical and Computer Engineering, The University of Auckland, Auckland, New Zealand, as a Research Fellow. In 2009, he joined the College of Automation, Chongqing University, where he is currently a Professor. His current research interests include nonlinear modeling and analysis, intelligent control, and wireless power transfer.

Jing Xiao was born in 1988. He received the master's degree in electrical engineering from Beijing Jiaotong University, Beijing, China, in 2013.

He is currently with Southern Power Grid Corporation, Wireless Power Transmission Joint Laboratory, Guangxi Power Grid Company Ltd., Nanning, China. His research interests include wireless power transmission technology.

Shaonan Chen received the B.S. and Ph.D. degrees in electronic engineering from Guangxi University, Nanning, China, in 2011 and 2016, respectively.

He is currently a Senior Power Grid Engineer with the Electric Power Research Institute, Guangxi Power Grid Company Ltd., Nanning. His major research interests include power system operation and reliability.